Modeling & Analysis

Overview

The gain scheduling methods of Chapter 1 that were judged to be the more promising and also offering the best background for further development were tested using two different benchmark examples. The first one is an analytic nonlinear model of the pitch axis dynamics of a highly manoeuvrable missile called the *Reichert Missile Benchmark (R'm'B)*. The second one is a tabulated nonlinear example of an atmospheric reentry vehicle *(ARV)* provided by the EADS Astrium Space Transportation corporation. This chapter gives the results obtained from the application of the first two steps of the Linearization-based Gain Scheduling Procedure (LBGS) of Section 1.3.1 (trimming and linearization) on these systems. Given that these two steps are common for any candidate for gain scheduling nonlinear system, the same analysis techniques were used and the results are presented in a similar way.

Chapter contents

4.1 The Reichert Benchmark Missile Model

The Reichert Missile Benchmark (R'm'B) was first presented in the control literature in the early 90's (see [112]) and has been the benchmark system for many works since, mostly due to the fact that it incorporates analytic formulas for the aerodynamic functions of the system. In this monograph, a similar but more recent version of the model appearing in [103] will be preferred.

4.1.1 Airframe Modeling

System dynamics

The nonlinear model of the R'm'B describes the longitudinal (or pitch) dynamics of a highly manoeuvrable missile airframe around its center of mass. The state vector x of the missile (see Fig. 4.1)[1] is its angle of attack α (in rad) and pitch rotational rate q (in rad$\cdot$s^{-1}). The command is the elevator deflection angle δ (in rad), the output is the vertical acceleration η (in g's) and its Mach number M is considered as an internal time varying parameter[2]. The state dynamics of the missile are given by:

$$\frac{d\alpha}{dt} = K_\alpha M C_{\mathrm{n}}(\alpha, M, \delta)\cos\alpha + q \tag{4.1}$$

$$\frac{dq}{dt} = K_{\mathrm{pr}} M^2 C_{\mathrm{m}}(\alpha, M, \delta) \tag{4.2}$$

whereas the output dynamics are:

$$\eta = K_\eta M^2 C_{\mathrm{n}}(\alpha, M, \delta)\,. \tag{4.3}$$

Aerodynamic functions

The lift force and pitching moment aerodynamic functions C_{n}, C_{m} are described by the following equations in standard notation:

$$C_{\mathrm{n}}(\alpha, M, \delta) = C_{\mathrm{n}\alpha}(\alpha, M)\,\alpha + C_{\mathrm{n}\delta}\delta \tag{4.4}$$

$$C_{\mathrm{m}}(\alpha, M, \delta) = C_{\mathrm{m}\alpha}(\alpha, M)\,\alpha + C_{\mathrm{m}\delta}\delta \tag{4.5}$$

with

$$C_{\mathrm{n}\alpha}(\alpha, M) = \left(\frac{180}{\pi}\right)^3 a_{\mathrm{n}}\alpha^2 + \left(\frac{180}{\pi}\right)^2 b_{\mathrm{n}}|\alpha| + \frac{180}{\pi}c_{\mathrm{n}}\left(2 - \frac{M}{3}\right) \tag{4.6}$$

$$C_{\mathrm{m}\alpha}(\alpha, M) = \left(\frac{180}{\pi}\right)^3 a_{\mathrm{m}}\alpha^2 + \left(\frac{180}{\pi}\right)^2 b_{\mathrm{m}}|\alpha| + \frac{180}{\pi}c_{\mathrm{m}}\left(-7 + \frac{8M}{3}\right) \tag{4.7}$$

and

$$C_{\mathrm{n}\delta} = \frac{180}{\pi}d_{\mathrm{n}} \tag{4.8}$$

$$C_{\mathrm{m}\delta} = \frac{180}{\pi}d_{\mathrm{m}}. \tag{4.9}$$

[1] The symbols $G_{\mathrm{m}}, G_{\mathrm{p}}$ correspond to the missile's center of mass and center of pressure.
[2] Explicit time dependence will be dropped when needed for the sake of simplicity.

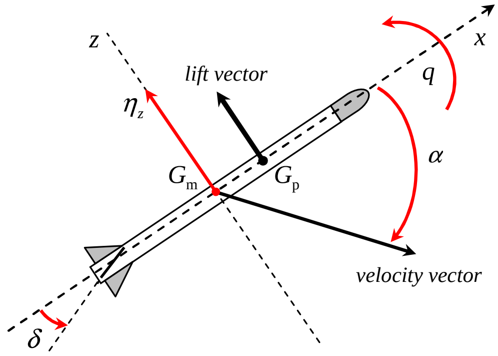

Figure 4.1: Missile pitch view

Table 4.1: Missile & actuator coefficients.

Name	Symbol	Expression	Value	Unit
Reference area	S	-	0.04088	m^2
Diameter	d	-	0.2286	m
Mass	m	-	204.02	kg
Moment of inertia	I_{yy}	-	247.44	$\mathrm{kg}\cdot\mathrm{m}^2$
Static pressure	P_0	-	46601.6	$\mathrm{N/m}^2$
Speed of sound	v_{s}	-	315.89	m/s
Drag coefficient	C_{a}	-	-0.3	-
Damping ratio	ξ	-	0.7	-
Natural frequency	ω_{a}	-	150	rad/s
-	K_α	$0.7P_0S/mv_{\mathrm{s}}$	0.02069	s^{-1}
-	K_{pr}	$0.7P_0Sd/I_{\mathrm{yy}}$	1.23194	s^{-2}
-	K_η	$0.7P_0S/mg$	0.66624	-
-	A_{x}	$0.7P_0SC_{\mathrm{a}}/I_{\mathrm{yy}}$	-1.96074	N/m
-	a_{n}	-	0.000103	deg^{-3}
-	b_{n}	-	-0.00945	deg^{-2}
-	c_{n}	-	-0.1696	deg^{-1}
-	d_{n}	-	-0.034	deg^{-1}
-	a_{m}	-	0.000215	deg^{-3}
-	b_{m}	-	-0.0195	deg^{-2}
-	c_{m}	-	0.051	deg^{-1}
-	d_{m}	-	-0.206	deg^{-1}

(i) The altitude is considered constant ($\simeq 6100m$).

The missile is considered to be operating during the terminal target intercepting phase with its engine thrust equal to zero and the Mach profile given by the following nonlinear differential equation: Mach trajectory

$$\frac{dM}{dt} = \frac{1}{v_s}\left(-|\eta|\sin|\alpha| + A_x M^2 \cos\alpha\right), \text{ with } M(0) = M_0. \tag{4.10}$$

The elevator fin is driven by an actuator modeled using the following second order filter (δ_c (in rad) is the control signal provided by the autopilot): Actuator dynamics

$$\frac{d^2\delta}{dt} + 2\xi\omega_a \frac{d\delta}{dt} + \omega_a^2\delta = \omega_a^2\delta_c. \tag{4.11}$$

The actuator and missile data coefficients are shown in Table 4.1. It should be noted that the latter are generally dependent on the flight altitude that is here considered as constant. The nonlinear mathematical model of the missile is valid for $-20° \leq \alpha \leq 20°$ and for $1.5 \leq M \leq 3$; these two variables forming its flight envelope.

The aerodynamic functions related to the angle of attack $C_{n\alpha}, C_{m\alpha}$ for $\alpha > 0$[3] are shown in Figs. 4.2a, 4.2b. It can be observed that there exists a significant variation of the functions values over α and M.

4.1.2 Trim Analysis

In this section the application of the first step of the Linearization-based Gain Scheduling Procedure (LBGS), concerning the missile trim control computation, will be detailed. The trim control δ_r is the rudder reference deflection angle needed in order to stabilize the missile around an equilibrium (or reference) point in the absence of external perturbations.

The equilibrium points can be parameterized as function of the angle of attack α or the vertical acceleration η, and the Mach number M. Each pair, α, M or η, M, forms the so-called scheduling vector ϱ used to describe the flight envelope of the missile.

4.1.2.1 Parametrization on α

The trim control $\delta(\varrho_r) = \delta_r$ for each value of the scheduling vector $\varrho_r = [\alpha_r \; M_r]^T$ inside the flight envelope specifications ($-20° \leq \alpha_r \leq 20°$ and $1.5 \leq M_r \leq 3$) can be calculated easily using Eqs. 4.2, 4.5, 4.7 and 4.9. Given that the airframe is on equilibrium for a given value ϱ_r, then $\frac{dq}{dt}\big|_r = 0$[4] and so: Trim input

$$\delta(\varrho_r) = -\frac{C_{m\alpha}(\varrho_r)}{C_{m\delta}}\alpha_r. \tag{4.12}$$

[3] For $\alpha < 0$ the functions are symmetric due to $|\alpha|$ entering in Eqs. 4.6, 4.7.

[4] The 'r' notation means calculation on a *reference-equilibrium* point.

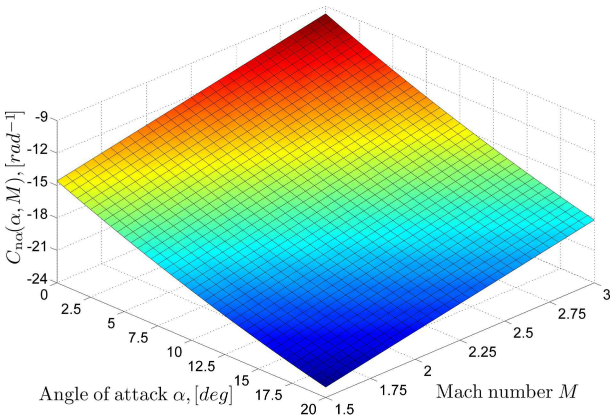

(a) *Lift aerodynamic function* $C_{n\alpha}$

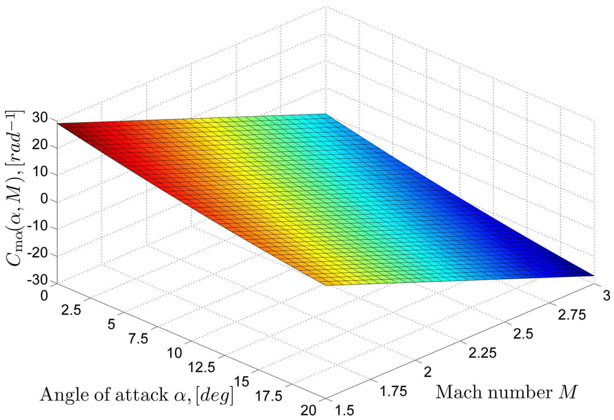

(b) *Pitching moment aerodynamic function* $C_{m\alpha}$

Figure 4.2: Missile aerodynamic function surfaces.

Furthermore, the corresponding trim values $q(\varrho_\mathrm{r}) = q_\mathrm{r}$ and $\eta(\varrho_\mathrm{r}) = \eta_\mathrm{r}$ can be calculated by letting $\frac{d\alpha}{dt}\big|_\mathrm{r} = 0$ and then substituting Eq. 4.12 into Eqs. 4.1 and 4.3 respectively:

Trim outputs

$$\begin{aligned} q(\varrho_\mathrm{r}) &= -K_\alpha M_\mathrm{r} C_\mathrm{n}(\alpha_\mathrm{r}, M_\mathrm{r}, \delta_\mathrm{r}) \cos\alpha_\mathrm{r} \\ &= -K_\alpha M_\mathrm{r} \Big[C_{\mathrm{n}\alpha}(\varrho_\mathrm{r}) - \frac{C_{\mathrm{n}\delta}}{C_{\mathrm{m}\delta}} C_{\mathrm{m}\alpha}(\varrho_\mathrm{r})\Big] \alpha_\mathrm{r} \cos\alpha_\mathrm{r} \end{aligned} \tag{4.13}$$

and

$$\begin{aligned} \eta(\varrho_\mathrm{r}) &= K_\eta M_\mathrm{r}^2 C_\mathrm{n}(\alpha_\mathrm{r}, M_\mathrm{r}, \delta_\mathrm{r}) \cos\alpha_\mathrm{r} \\ &= K_\eta M_\mathrm{r}^2 \Big[C_{\mathrm{n}\alpha}(\varrho_\mathrm{r}) - \frac{C_{\mathrm{n}\delta}}{C_{\mathrm{m}\delta}} C_{\mathrm{m}\alpha}(\varrho_\mathrm{r})\Big] \alpha_\mathrm{r}. \end{aligned} \tag{4.14}$$

The results (3D and contour maps) of the trim procedure are visualized in Figs. 4.3a-4.3f in the next page. It may be observed that for positive values of the angle of attack, the corresponding trim control is negative, the trim pitch rate positive, and the trim output negative. For negative angles of attack the results are of course symmetric.

4.1.2.2 Parametrization on η

The parametrization of the trim control using the angle of attack α described previously (see Section 4.1.2.1) is not preferable since α is usually not measured. The variable that is actually measured (using accelerometers) is the output of the plant η. As a result the trim control δ_r should be re-parameterized in terms of a new scheduling vector $\varrho = [\eta\ M]^T$ for every equilibrium point. To do this, the following procedure is used:

Trimming algorithm

1. *Trim Control:* Express the trim control δ_r as a function of the new scheduling vector $\varrho_\mathrm{r} = [\eta_\mathrm{r}\ M_\mathrm{r}]^T$ and the corresponding trim value for the angle of attack $\alpha(\varrho_\mathrm{r}) = \alpha_\mathrm{r}$ that is not known for the moment. To do this use Eq. 4.3 along with Eqs. 4.4, 4.6 and 4.8.

Trim input

$$\delta(\eta_\mathrm{r}, M_\mathrm{r}, \alpha_\mathrm{r}) = \frac{\dfrac{\eta_\mathrm{r}}{K_\eta M_\mathrm{r}^2} - C_{\mathrm{n}\alpha}(\alpha_\mathrm{r}, M_\mathrm{r})\alpha_\mathrm{r}}{C_{\mathrm{n}\delta}} \tag{4.15}$$

2. *Angle of Attack:* Supposing that the system is on equilibrium (briefly $\dot{x}|_\mathrm{r} \triangleq 0$ and so the left hand sides of Eqs. 4.1, 4.2 go to zero), replace $\delta(\eta_\mathrm{r}, M_\mathrm{r}, \alpha_\mathrm{r})$ of Eq. 4.15 into the pitch rate equation (see Eq. 4.2) obtaining:

$$\begin{aligned} 0 &= C_\mathrm{m}(\alpha_\mathrm{r}, M_\mathrm{r}, \delta_\mathrm{r}) \\ &= C_{\mathrm{m}\alpha}(\alpha_\mathrm{r}, M_\mathrm{r})\alpha_\mathrm{r} + C_{\mathrm{m}\delta}\delta(\eta_\mathrm{r}, M_\mathrm{r}, \alpha_\mathrm{r}) \\ &= C_{\mathrm{m}\alpha}(\alpha_\mathrm{r}, M_\mathrm{r})\alpha_\mathrm{r} + \frac{C_{\mathrm{m}\delta}}{C_{\mathrm{n}\delta}}\Big(\frac{\eta_\mathrm{r}}{K_\eta M_\mathrm{r}^2} - C_{\mathrm{n}\alpha}\alpha_\mathrm{r}\Big). \end{aligned} \tag{4.16}$$

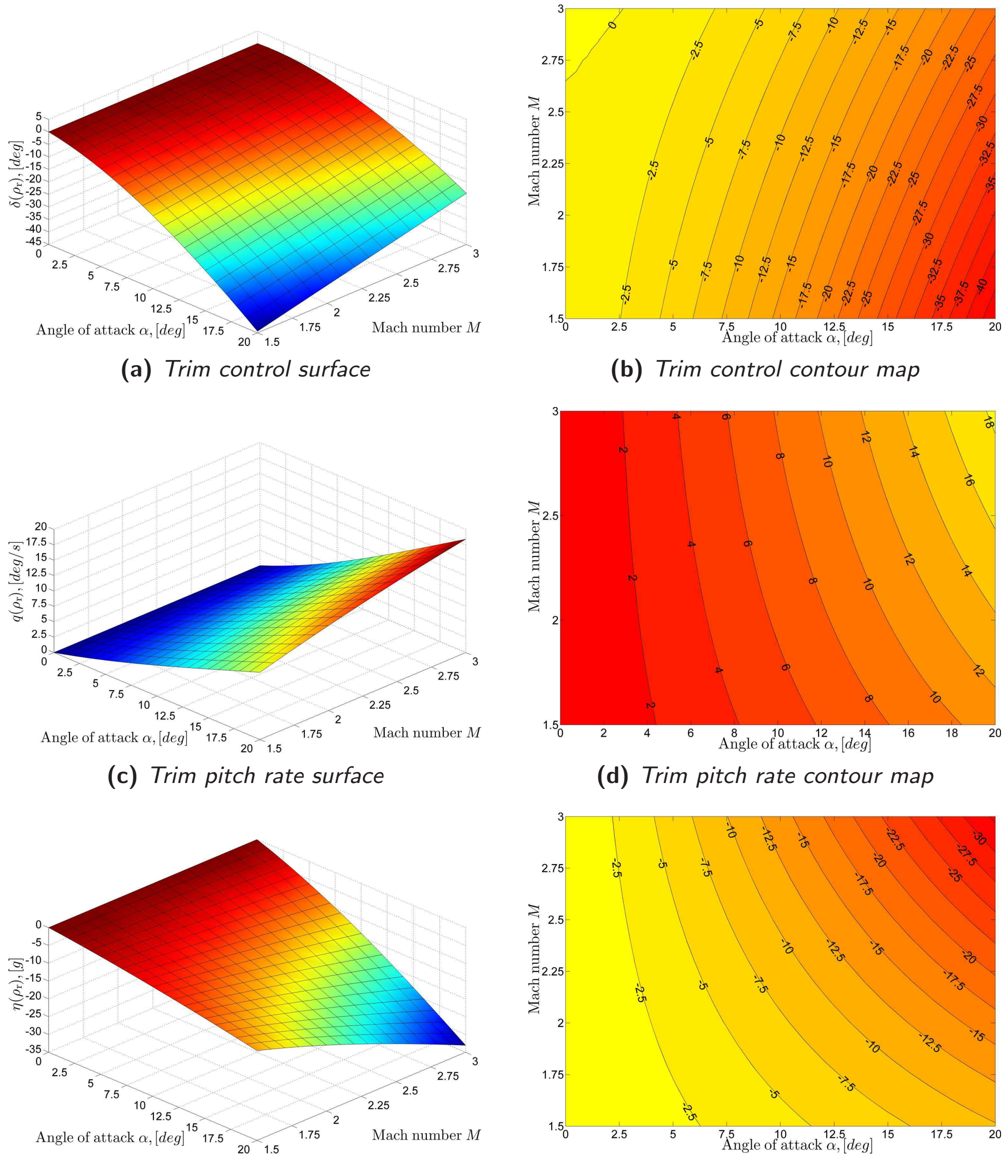

(a) *Trim control surface* **(b)** *Trim control contour map*

(c) *Trim pitch rate surface* **(d)** *Trim pitch rate contour map*

(e) *Trim vertical acceleration surface* **(f)** *Trim vertical acceleration contour map*

Figure 4.3: Missile trim results -*parametrization on* α

From the last expression, the following third order polynomial equation for α_r as a function of the scheduling vector variables $\eta_\mathrm{r}, M_\mathrm{r}$ is taken:

$$\left(a_\mathrm{m} - \frac{d_\mathrm{m}}{d_\mathrm{n}} a_\mathrm{n}\right)\left(\frac{180}{\pi}\alpha_\mathrm{r}\right)^3 + \mathrm{sgn}(\alpha_\mathrm{r})\left(b_\mathrm{m} - \frac{d_\mathrm{m}}{d_\mathrm{n}} b_\mathrm{n}\right)\left(\frac{180}{\pi}\alpha_\mathrm{r}\right)^2 + \\ + \left[c_\mathrm{m}\left(-7 + \frac{8M_\mathrm{r}}{3}\right) - \frac{d_\mathrm{m}}{d_\mathrm{n}} c_\mathrm{n}\left(2 - \frac{M_\mathrm{r}}{3}\right)\right]\left(\frac{180}{\pi}\alpha_\mathrm{r}\right) + \frac{d_\mathrm{m}}{d_\mathrm{n} K_\eta}\frac{\eta_\mathrm{r}}{M_\mathrm{r}^2} = 0 \tag{4.17}$$

or in a more compact, ϱ_r-dependent form:

$$k_1 \alpha_\mathrm{r}^3 + k_2\,\mathrm{sgn}(\alpha_\mathrm{r})\alpha_\mathrm{r}^2 + k_3(\varrho_\mathrm{r})\alpha_\mathrm{r} + k_4(\varrho_\mathrm{r}) = 0. \tag{4.18}$$

Finally, because of the fact that $\mathrm{sgn}(\alpha_\mathrm{r}) = -\mathrm{sgn}(\eta_\mathrm{r})$ (see Figs. 4.3e, 4.3f), the last equation can be written: `Trim AoA`

$$k_1 \alpha_\mathrm{r}^3 - k_2\,\mathrm{sgn}(\eta_\mathrm{r})\alpha_\mathrm{r}^2 + k_3(\varrho_\mathrm{r})\alpha_\mathrm{r} + k_4(\varrho_\mathrm{r}) = 0. \tag{4.19}$$

The previous polynomial equation can be solved for α_r, for each value of ϱ_r using either the classic method of Cardano or numerical root finding methods. In either case one will get three solutions for α_r; however only one has a physical sense[5]. For every ϱ_r, one solution has always the opposite sign than expected whereas another one violates the flight envelope constraints taken over α (see Section 4.1.2.1). The acceptable solution is shown in Figs. 4.4a, 4.4b[6].

3. *Pitch Rate:* Since the trim value α_r is computed by solving Eq. 4.19 for every ϱ_r, the corresponding trim control δ_r may be calculated by replacing α_r into Eq. 4.15. In addition, the trim pitch rate values can be also found by replacing $\alpha_\mathrm{r}, \delta_\mathrm{r}$ into Eq. 4.1 given that $\frac{d\alpha}{dt}\big|_\mathrm{r} = 0$: `Trim pitch rate`

$$q_\mathrm{r} = -K_\alpha M_\mathrm{r} C_\mathrm{n}(\alpha_\mathrm{r}, M_\mathrm{r}, \delta_\mathrm{r}) \cos\alpha_\mathrm{r}. \tag{4.20}$$

The trim control and trim pitch rate when using the η-parametrization are shown in Figs. 4.4c-4.4f.

The trim control $\delta(\varrho_\mathrm{r})$ is needed as a necessary part of a gain-scheduled control law in order to ensure proper reference point tracking. For implementation of such control laws, on line computation of $\delta(\varrho_\mathrm{r})$ is unrealistic since it involves real time solution of the aforementioned polynomial equation (see Eq. 4.19). For this reason, the trim control is calculated off-line for a sufficient number of points and the results are stored in a look-up table. Linear interpolation is then used to provide an appropriate value for every other point ϱ_r of the flight envelope[7].

[5] For the singular case $\eta_\mathrm{r} = 0$, the solution considered is $\alpha_\mathrm{r} = 0$.
[6] Only positive values for η_r are considered; for negative ones the results are symmetric.
[7] Here a total number of $66 \times 66 = 4356$ points was used.

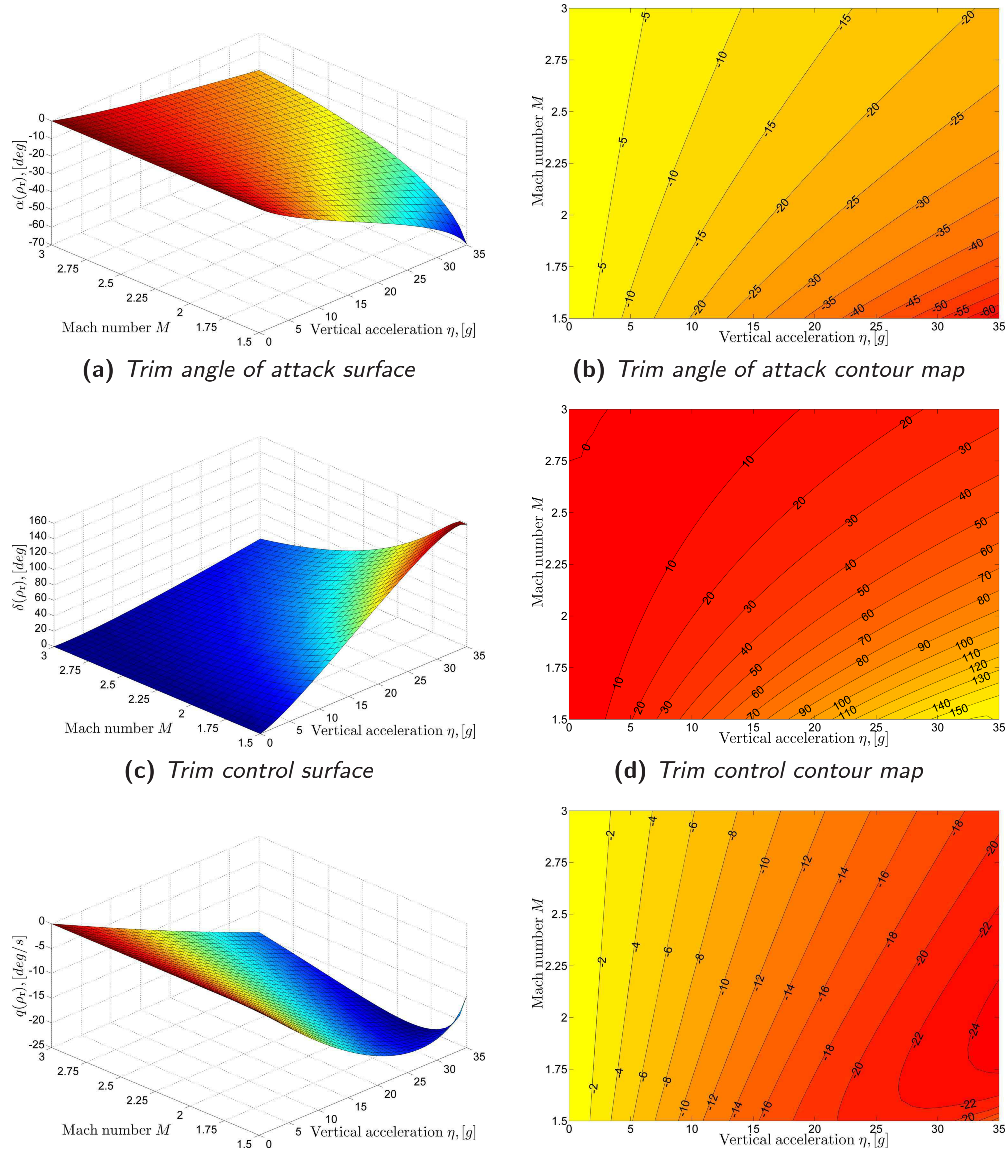

(a) *Trim angle of attack surface* **(b)** *Trim angle of attack contour map*

(c) *Trim control surface* **(d)** *Trim control contour map*

(e) *Trim pitch rate surface* **(f)** *Trim pitch rate contour map*

Figure 4.4: Missile trim results - *parametrization on* η

4.1.2.3 Flight Envelope Analysis

Most works concerning the R'm'B model lack a thorough analysis of the missile's flight envelope (see [17, 36, 55, 81, 99]). This is probably due to the fact that the flight envelope is directly parameterized using α, M and not η, M that is more realistic, since α is not available for feedback[8]. However, all the operating constraints are initially imposed on the angle of attack and the Mach, as presented in Section 4.1.1, defining the corresponding $[\alpha, M]$-dependent flight envelope $\mathbf{\Gamma}_{\text{fe}}^{[\alpha,M]}$:

$[\alpha, M]$ `flight envelope`

$$\mathbf{\Gamma}_{\text{fe}}^{[\alpha,M]} : \left[|\alpha| \leq 20°, 1.5 \leq M \leq 3\right]. \tag{4.21}$$

The flight envelope can be re-parameterized in terms of η, M, using the analysis of Section 4.1.2. The result is a non convex hull as it can be seen in Fig. 4.4b (for $\eta_{\text{r}} > 0$), with the isoline $\alpha = -20°$ setting the right border of the envelope. An analytic expression $\eta_{\text{fe}}(M)$ for this isoline can be easily found by setting $\alpha = -20°$ in Eq. 4.17 (symmetric results are obtained for for $\eta_{\text{r}} < 0$):

$$\eta_{\text{fe}}(M) \simeq -0.454M^3 + 5.035M^2. \tag{4.22}$$

The $[\eta, M]$-dependent flight envelope $\mathbf{\Gamma}_{\text{fe}}^{[\eta,M]}$ is now given by Eq. 4.23 and is visualized in Fig. 4.5 (yellow surface). A convex linear approximation $\mathbf{\Gamma}_{\text{fe,lin}}^{[\eta,M]}$ (yellow plus red surface) will be used from now on to simplify the shape of the flight envelope in order to make the task of interpolation easier and is given by Eq. 4.24:

$[\eta, M]$ `flight envelopes`

$$\mathbf{\Gamma}_{\text{fe}}^{[\eta,M]} : \left[0 \leq \eta \leq \eta_{\text{fe}}(M), 1.5 \leq M \leq 3\right] \tag{4.23}$$

$$\mathbf{\Gamma}_{\text{fe,lin}}^{[\eta,M]} : \left[0 \leq \eta \leq \eta_{\text{fe,lin}}(M), 1.5 \leq M \leq 3\right] \tag{4.24}$$

with

$$\eta_{\text{fe,lin}}(M) \simeq 15.506M - 13.462. \tag{4.25}$$

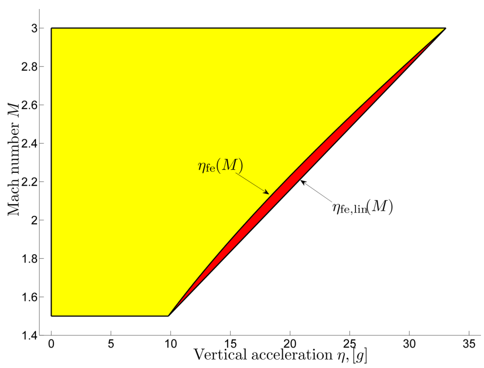

Figure 4.5: Missile flight envelope

[8]In practice, an estimator could be used to obtain α but this results to greater complexity.

The discussion of this section showed that if a careful analysis of the operating domain is not performed according to the initial nonlinear system constraints, redundancy will occur. Indeed, if a rectangular flight envelope had been used as in Section 4.1.2, the surface redundancy with respect to $\mathbf{\Gamma}_{\text{fe}}^{[\eta,M]}$ would have been around 60%, whereas with the linear approximation $\mathbf{\Gamma}_{\text{fe,lin}}^{[\eta,M]}$ it is only 3.6%. This surface redundancy is particularly important for a gain-scheduled controller since it can significantly augment the number of synthesis points and hence the interpolation complexity.

4.1.3 System Linearization

After the analysis of Sections 4.1.2.1-4.1.2.3 and the parametrization of the equilibrium points of the missile in terms of the scheduling vector $\varrho = [\eta\ M]^T$, the second step of the Linearization-based Gain Scheduling procedure (LBGS) concerning linearization will now be detailed according to the standard analysis of Section 1.3.1.

4.1.3.1 LTI Models

LTI models

The goal here is to provide an LPV model of the missile's nonlinear dynamics (see Eqs. 4.1-4.9) smoothly parameterized by the scheduling vector $\varrho = [\eta\ M]^T$ with $\varrho \in \mathbf{\Gamma}_{\text{fe,lin}}^{[\eta,M]}$ and the corresponding equilibrium manifold information obtained from the trim analysis. For notational simplicity, frozen instances of the LPV model will be considered (with 'r' meaning frozen equilibrium-reference operation):

$$\dot{x}_\delta = \mathbf{A}(\varrho_\text{r})x_\delta + \mathbf{B}(\varrho_\text{r})\delta_\delta \tag{4.26}$$

$$y_\delta = \mathbf{C}(\varrho_\text{r})x_\delta + \mathbf{D}(\varrho_\text{r})\delta_\delta \tag{4.27}$$

with $x = [\alpha\ q]^T, y = [\eta\ q]^T$ and

$$x_\delta = x - x(\varrho_\text{r}) \tag{4.28}$$

$$\delta_\delta = \delta - \delta(\varrho_\text{r}) \tag{4.29}$$

$$y_\delta = y - y(\varrho_\text{r}). \tag{4.30}$$

The linear systems' matrices are computed using Jacobian linearization of the initial nonlinear system dynamics, for any desired value ϱ_r of the scheduling vector inside the flight envelope:[9]

$$\left[\begin{array}{c|c} \mathbf{A}(\varrho_\text{r}) & \mathbf{B}(\varrho_\text{r}) \\ \hline \mathbf{C}(\varrho_\text{r}) & \mathbf{D}(\varrho_\text{r}) \end{array}\right] \triangleq \begin{bmatrix} \nabla_{x,\text{r}} f_x & \nabla_{\delta,\text{r}} f_x \\ \nabla_{x,\text{r}} h_y & \nabla_{\delta,\text{r}} h_y \end{bmatrix} \tag{4.31}$$

[9]For notational simplicity, $f_x = [f_\alpha, f_q]^T : \mathbb{R}^4 \to \mathbb{R}^2$ and $h_y = [h_\eta, q]^T : \mathbb{R}^3 \to \mathbb{R}$ are the nonlinear functions of the missile's state and output dynamics (Eqs. 4.1-4.3).

with: Jacobians

$$\nabla_x f_x = \begin{pmatrix} \nabla_\alpha f_\alpha & \nabla_q f_\alpha \\ \nabla_\alpha f_q & \nabla_q f_q \end{pmatrix} \tag{4.32}$$

$$\nabla_\delta f_x = \begin{pmatrix} \nabla_\delta f_\alpha \\ \nabla_\delta f_q \end{pmatrix} \tag{4.33}$$

$$\nabla_x h_y = \begin{pmatrix} \nabla_\alpha h_\eta & \nabla_q h_\eta \\ 0 & 1 \end{pmatrix} \tag{4.34}$$

$$\nabla_\delta h_y = \begin{pmatrix} \nabla_\delta h_\eta \\ 0 \end{pmatrix}. \tag{4.35}$$

The partial derivatives entering all the previous equations can be explicitly computed using the following formulas[10]:

$$\nabla_\alpha f_\alpha = K_\alpha M \Big[\cos\alpha\big(C_{\mathrm{n}\alpha} + \alpha \nabla_\alpha C_{\mathrm{n}\alpha}\big) - \sin\alpha C_{\mathrm{n}}\Big] \tag{4.36}$$

$$\nabla_q f_\alpha = 1 \tag{4.37}$$

$$\nabla_\alpha f_q = K_{\mathrm{pr}} M^2 \big(C_{\mathrm{m}\alpha} + \alpha \nabla_\alpha C_{\mathrm{m}\alpha}\big) \tag{4.38}$$

$$\nabla_q f_q = 0 \tag{4.39}$$

$$\nabla_\delta f_\alpha = K_\alpha M C_{\mathrm{n}\delta} \cos\alpha \tag{4.40}$$

$$\nabla_\delta f_q = K_{\mathrm{pr}} C_{\mathrm{m}\delta} M^2 \tag{4.41}$$

$$\nabla_\alpha h_\eta = K_\eta M^2 \big(C_{\mathrm{n}\alpha} + \alpha \nabla_\alpha C_{\mathrm{n}\alpha}\big) \tag{4.42}$$

$$\nabla_q h_\eta = 0 \tag{4.43}$$

$$\nabla_\delta h_\eta = K_\eta C_{\mathrm{m}\delta} M^2. \tag{4.44}$$

The partial derivatives (computed using Eqs. 4.36-4.44) of the LTI models (see Eqs. 4.26, 4.27) are not only dependent on M but also on α, δ; parameters that not belong to the scheduling vector ϱ. However, given that these derivatives are computed at desired operating-equilibrium points and the corresponding equilibrium values $\alpha_{\mathrm{r}}, \delta_{\mathrm{r}}$ can be parameterized as a function of the scheduling vector ϱ_{r} (according to the analysis of Sections 4.1.2.2, 4.1.2.3), it can be clearly seen that these LTI models *are fully parameterized by the scheduling vector only.*

Regrouping the above results, all linear time invariant, scheduling vector dependent (with $\varrho \in \boldsymbol{\Gamma}^{[\eta,M]}_{\mathrm{fe,lin}}$) models of the R'm'B can be written in the following transfer function and state space forms (see Eqs. 4.45, 4.46):

$$\mathcal{S}_{\mathrm{LPV}}(\varrho_{\mathrm{r}}) \overset{\mathrm{tf}}{\vdots} \quad \left\{ \begin{bmatrix} \eta_\delta(s) \\ q_\delta(s) \end{bmatrix} = \begin{bmatrix} G_\eta(s) \\ G_q(s) \end{bmatrix} \delta_\delta = G(s)\delta_\delta. \right. \tag{4.45}$$

[10]The aerodynamic functions $C_{\mathrm{n}}, C_{\mathrm{n}\alpha}, C_{\mathrm{m}\alpha}$ dependency on α, M, δ is omitted for notational simplicity.

$$\mathcal{S}_{\mathrm{LPV}}(\varrho_{\mathrm{r}}) \overset{\mathrm{ss}}{:} \quad \begin{cases} \begin{pmatrix} \dot{\alpha}_\delta \\ \dot{q}_\delta \end{pmatrix} = \begin{pmatrix} \nabla_{\alpha,\mathrm{r}} f_\alpha & 1 \\ \nabla_{\alpha,\mathrm{r}} f_q & 0 \end{pmatrix} \begin{pmatrix} \alpha_\delta \\ q_\delta \end{pmatrix} + \begin{pmatrix} \nabla_{\delta,\mathrm{r}} f_\alpha \\ \nabla_{\delta,\mathrm{r}} f_q \end{pmatrix} \delta_\delta \\ \begin{pmatrix} \eta_\delta \\ q_\delta \end{pmatrix} = \begin{pmatrix} \nabla_{\alpha,\mathrm{r}} h_\eta & 0 \\ 0 & 1 \end{pmatrix} \begin{pmatrix} \alpha_\delta \\ q_\delta \end{pmatrix} + \begin{pmatrix} \nabla_{\delta,\mathrm{r}} h_\eta \\ 0 \end{pmatrix} \delta_\delta \end{cases} \tag{4.46}$$

Missile transfer functions

The matrix transfer function $G(s) = C(sI - A)^{-1}B + D$ presents totally two poles, two zeros for the η-channel and one zero for the q-channel I/O transfer functions as seen from the following relation:

$$G = \begin{bmatrix} G_\eta \\ G_q \end{bmatrix} = \frac{\begin{bmatrix} D_{11}s^2 + (C_{11}B_{11} - A_{11}D_{11})s + C_{11}B_{21} - A_{21}D_{11} \\ -B_{21}s + A_{21}B_{11} - B_{21}A_{11} \end{bmatrix}}{s^2 - A_{11}s - A_{21}}. \tag{4.47}$$

The elements of the state space matrices $\mathbf{A}, \mathbf{B}, \mathbf{C}$ and $\mathbf{D}$, depending on the scheduling vector $\varrho = [\eta \;\, M]^T$, make the values of the zeros and poles of the aforementioned I/O transfer functions varying over the flight envelope. This necessitate a comprehensive stability and dynamics analysis of the linear systems $\mathcal{S}_{\mathrm{LPV}}(\varrho_{\mathrm{r}})$ for every value of the scheduling vector that will shed some light on the stability of the initial nonlinear plant. These six scheduling vector-dependent elements $A_{11}, A_{21}, B_{11}, B_{21}, C_{21}, D_{11}$ are visualized in Figs 4.6a-4.6f.

4.1.3.2 Stability Analysis

The local stability properties of the missile nonlinear dynamics (see Eqs. 4.1-4.2) can be investigated using the well-known Lyapunov's indirect method. For a given reference-equilibrium state x_{r} parameterized in terms of the scheduling vector $\varrho_{\mathrm{r}} = [\eta_{\mathrm{r}} \;\, M_{\mathrm{r}}]^T$, the eigenvalues of $\mathbf{A}(\varrho_{\mathrm{r}})$ provide the information if the missile is locally stable around this equilibrium point. The eigenvalues and the corresponding stability condition are:

Eigenvalues

$$\lambda_{1,2}(\varrho_{\mathrm{r}}) = \frac{\nabla_{\alpha,\mathrm{r}} f_\alpha \pm \sqrt{\left(\nabla_{\alpha,\mathrm{r}} f_\alpha\right)^2 + 4\nabla_{\alpha,\mathrm{r}} f_q}}{2} \tag{4.48}$$

Stability condition: The linear missile dynamics are stable iff for $\varrho_{\mathrm{r}} \in \mathbf{\Gamma}^{[\eta,M]}_{\mathrm{fe,lin}}$,

$$\begin{aligned} \nabla_{\alpha,\mathrm{r}} f_\alpha &< 0 \\ \nabla_{\alpha,\mathrm{r}} f_q &< 0. \end{aligned} \tag{4.49}$$

From Fig. 4.6a it can be seen that the first stability condition is always satisfied for all the flight envelope; however the second one not always (see Fig. 4.6c). Using Eq. 4.38 it can be rewritten as a condition over $C_{\mathrm{m}\alpha}$:

$$C_{\mathrm{m}\alpha,\mathrm{r}} < -\alpha_{\mathrm{r}} \nabla_{\alpha,\mathrm{r}} C_{\mathrm{m}\alpha}. \tag{4.50}$$

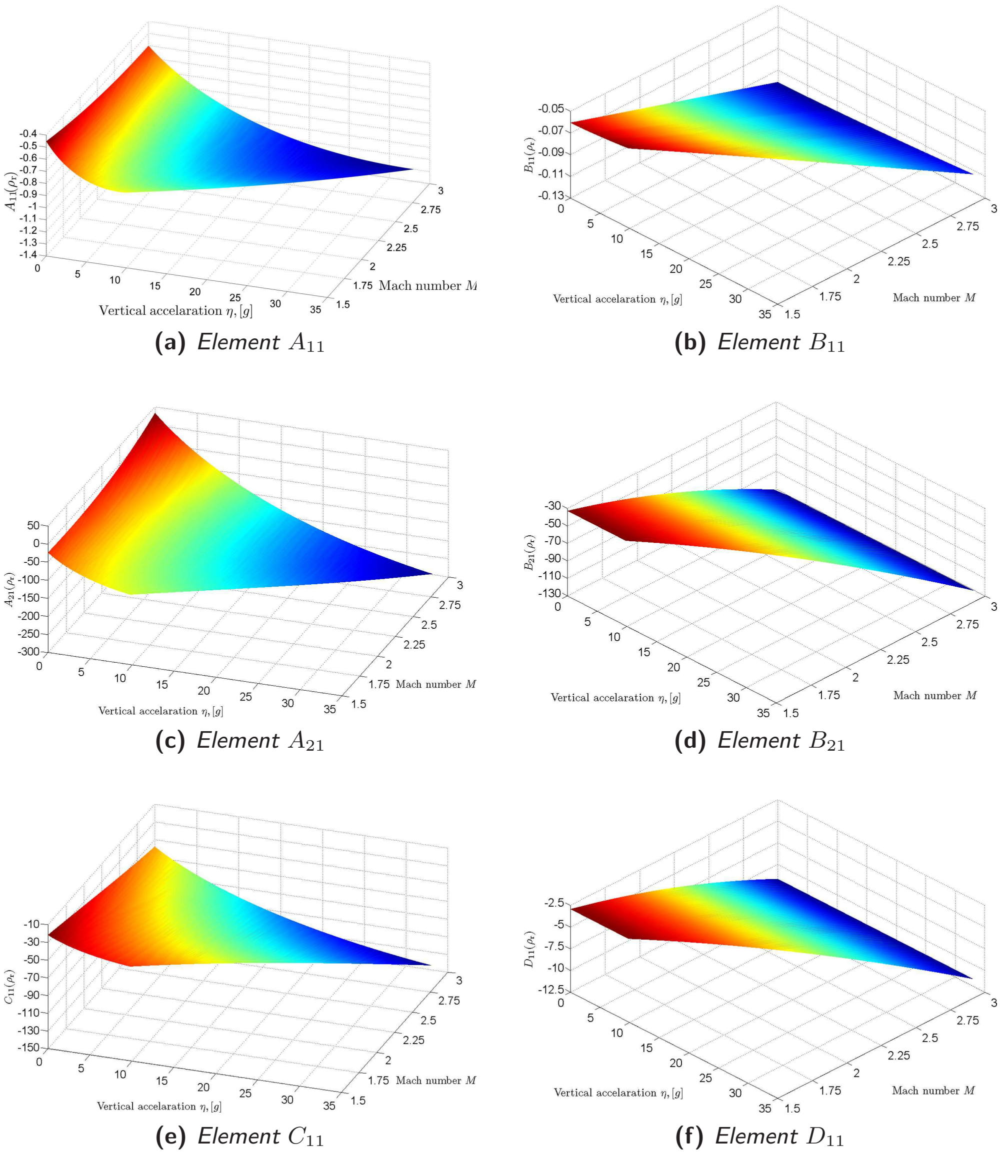

(a) *Element* A_{11} **(b)** *Element* B_{11}

(c) *Element* A_{21} **(d)** *Element* B_{21}

(e) *Element* C_{11} **(f)** *Element* D_{11}

Figure 4.6: Missile LTI system matrix elements

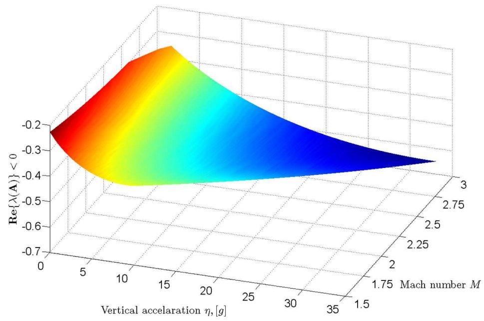

(a) *Stable eigenvalues' real part*

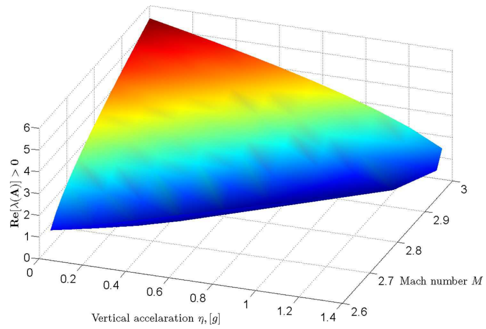

(b) *Unstable eigenvalues' real part*

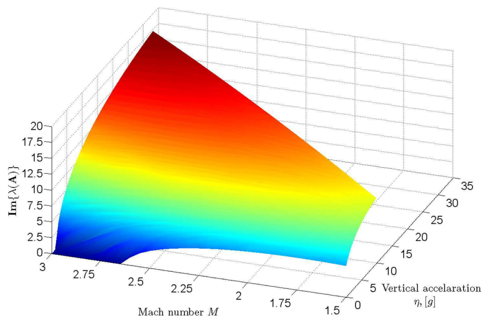

(c) *Eigenvalues' absolute imaginary value*

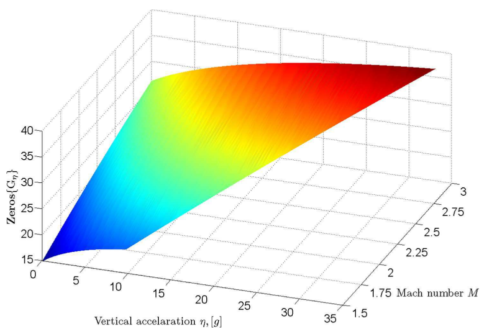

(d) G_η *transmission zeros (absolute value)*

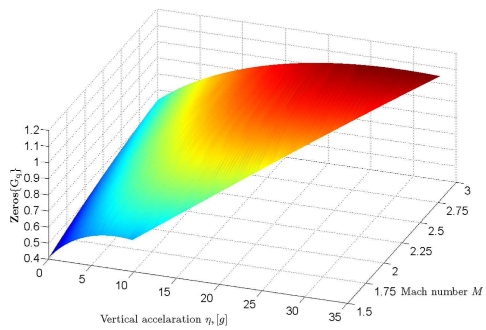

(e) G_q *transmission zeros*

Figure 4.7: Missile linearization results - *eigenvalues, transmission zeros*

The right hand side of Eq. 4.50 is always positive since by observing Fig. 4.2a, the slope of the aerodynamic function is always negative for $\alpha > 0$ (symmetry exists always for $\alpha < 0$). Thus it can be said that roughly, the airframe is stable iff $C_{\mathrm{m}\alpha} < 0$ but this is not totally correct. This previous type of stability analysis based on the sign of $C_{\mathrm{m}\alpha}$ is rather classical (see [77]) and is based on the fact that if for a given equilibrium angle of attack α_{r} and a corresponding trim input δ_{r}, the variation on the pitching moment due to the aerodynamic forces with respect to the center of gravity, caused by an external perturbation and forcing the plant to a new $\alpha = \alpha_{\mathrm{r}} + \Delta\alpha$, tends to bring the angle of attack to its initial equilibrium value, then the airframe is stable. `Stability discussion`

The full stability conditions (see Eq. 4.49) are given as a function of α and it is difficult to translate them directly on η in order to symbolically calculate the boundaries of the unstable region. The symbolical calculations can be avoided and stability could be studied by iteratively computing the sign of the eigenvalues of the missile linearized dynamics for a fixed gridding of the flight envelope. Thus a good approximation of the unstable subregion $\mathbf{\Gamma}_{\text{fe,un}}$ (with $\mathbf{\Gamma}_{\text{fe,lin}}^{[\eta,M]} \subset \mathbf{\Gamma}_{\text{fe,lin}}$) can be found (see Fig. 4.8). The surface percentage of $\mathbf{\Gamma}_{\text{fe,un}}$ with respect to $\mathbf{\Gamma}_{\text{fe,lin}}^{[\eta,M]}$ and $\mathbf{\Gamma}_{\text{fe}}^{[\eta,M]}$ is 0.82% and 0.79% respectively.

The linear analysis of the missile's nonlinear dynamics can also provide some very interesting insight results visualized in the following pages. In Figs. 4.7a, 4.7b, the amplitude of the real part of the LTI plants' eigenvalues for both the stable and unstable parts of $\mathbf{\Gamma}_{\text{fe,lin}}^{[\eta,M]}$ is visualized whereas in Fig. 4.7c the imaginary part is displayed. The evolution of the transmission zeros of $G(s)$ (see Eq. 4.47) is also shown in Figs 4.7d, 4.7e. `LTI models properties`

Finally, in Figs. 4.9a-4.9h the Bode diagrams and the I/O pole-zero maps of $G = [G_\eta \;\; G_q]^T$ are visualized for four different values of the Mach. Two things may be observed: first, the poles of the system are stable but badly damped (except for some unstable cases for $M = 3$, corresponding to $\mathbf{\Gamma}_{\text{fe,un}}$) and second, the plant has non-minimal phase transmission zeros for G_η whereas the zeros of G_q remain stable. In general it can be remarked that all these characteristics of the LTI plants are considerably varying over the flight envelope.

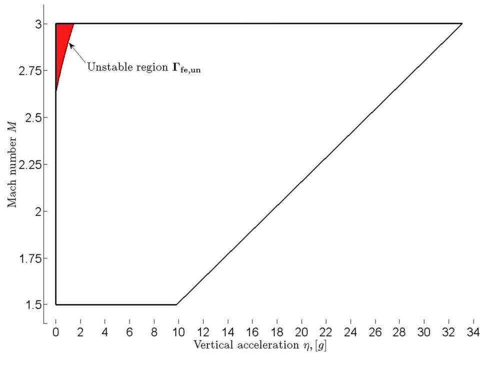

Figure 4.8: Missile flight envelope unstable part

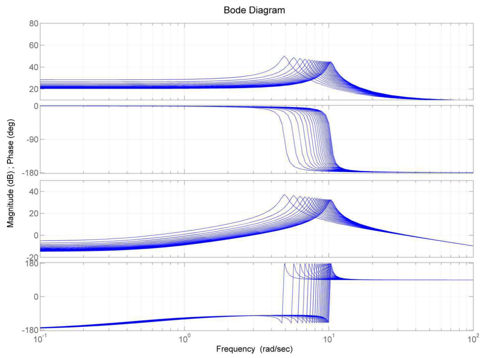

(a) $M = 1.5$

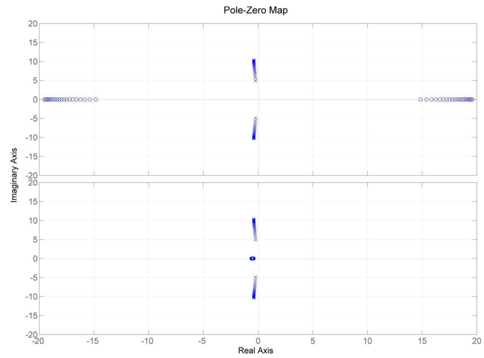

(b) $M = 1.5$

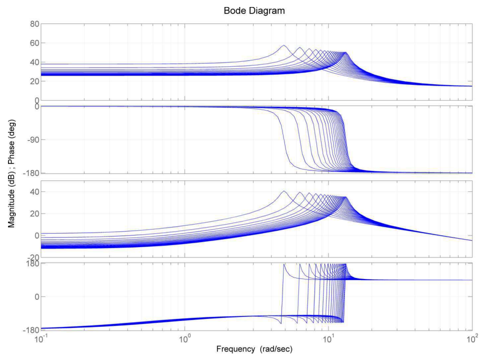

(c) $M = 2$

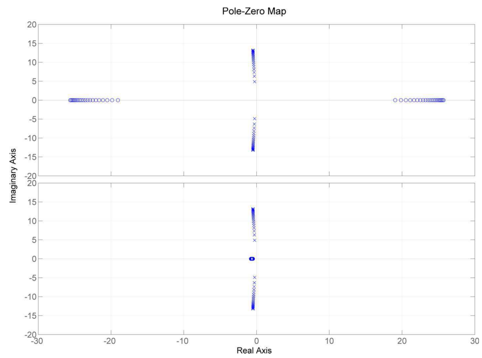

(d) $M = 2$

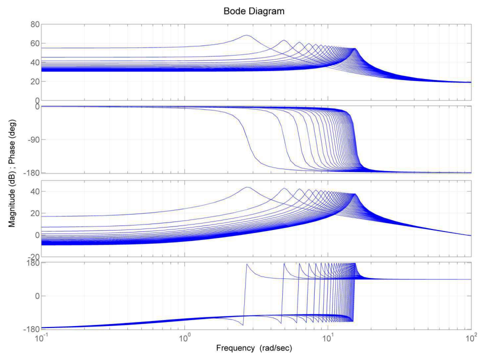

(e) $M = 2.5$

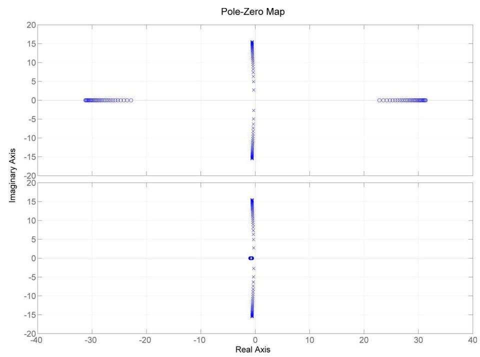

(f) $M = 2.5$

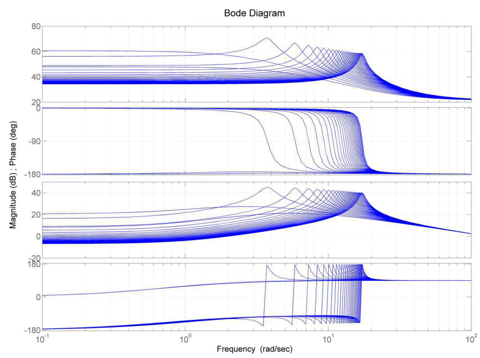

(g) $M = 3$

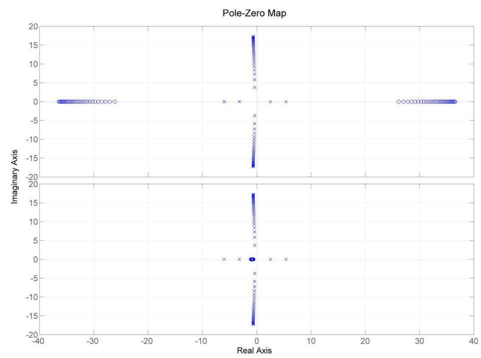

(h) $M = 3$

Figure 4.9: Missile Bode and Pole-zero maps of G_η, G_q

4.2 The ARV Benchmark Model

The second system considered in this work is an atmospheric re-entry vehicle example (ARV) provided by EADS ASTRIUM Space Transportation corporation. It is used to validate the techniques developed during this thesis and the results given are by no means representing real situations; however they are accurate enough to provide insight into the control methods presented in the next chapters.

4.2.1 Airframe Modeling

System dynamics

The nonlinear model of the vehicle[11] presented here describes its longitudinal motion during the atmospheric re-entry phase (a pitch view is shown in Fig. 4.10). The state x here is once again the angle of attack α (in rad) and the pitch rate q (in $\mathrm{rad}\cdot\mathrm{s}^{-1}$). Two control signals $\delta_{\mathrm{el}}, \delta_{\mathrm{er}}$ (in rad) representing the left and right tail elevator deflections are available to manipulate the vehicle's pitch and roll motion. The deflections are symmetric for pitch control (defining the pitch control signal δ_{e}) and antisymmetric for roll control; here only the first will be considered and is defined as[12]:

$$\delta_{\mathrm{e}} = \frac{1}{2}(\delta_{\mathrm{el}} + \delta_{\mathrm{er}}). \tag{4.51}$$

The pitch rate dynamics of the vehicle are dependent on the Mach number M following a predefined time trajectory (Fig. 4.12a), on the dynamic pressure Q (in N/m^2) depending on the Mach (Fig. 4.12b) and on the physical parameters of the vehicle (Table 4.2). The state dynamics are:

$$\frac{d\alpha}{dt} = q \tag{4.52}$$

$$\frac{dq}{dt} = \frac{SlQ}{I_{\mathrm{yy}}} C_{\mathrm{m}}(\alpha, M, \delta_{\mathrm{e}}) \tag{4.53}$$

where the pitching moment aerodynamic function C_{m} is defined as:

$$C_{\mathrm{m}}(\alpha, M, \delta_{\mathrm{e}}) = C_{\mathrm{m0}}(\alpha, M) + C_{\mathrm{me}}(\alpha, M)\delta_{\mathrm{e}}. \tag{4.54}$$

Flight envelope

The highly nonlinear aerodynamic function derivatives $C_{\mathrm{m0}}, C_{\mathrm{me}}$ are not available in symbolic form as in the missile but are rather tabulated for various points of the vehicle flight envelope (Figs. 4.11a, 4.11b). The latter is parameterized in terms of the angle of attack and the Mach number, thus the scheduling vector taken here is $\varrho = [\alpha\ M]^T$. The flight envelope $\mathbf{\Gamma}_{\mathrm{fe}}^{[\alpha,M]}$ is defined as:

$$\mathbf{\Gamma}_{\mathrm{fe}}^{[\alpha,M]} : \left[30^\circ \leq \alpha \leq 50^\circ, 4 \leq M \leq 26\right]. \tag{4.55}$$

[11] Real values for several parameters are not given for confidentiality reasons.
[12] Once more time dependence is omitted to simplify the equations.

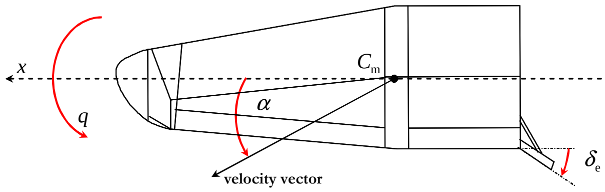

Figure 4.10: The ARV vehicle

Table 4.2: Vehicle & actuator coefficients

Name	Symbol	Unit
Damping ratio	ξ	-
Natural frequency	ω_{a}	rad/s
Reference area	S	m^2
Reference length	l	m
Moment of Inertia	I_{yy}	kgm^2

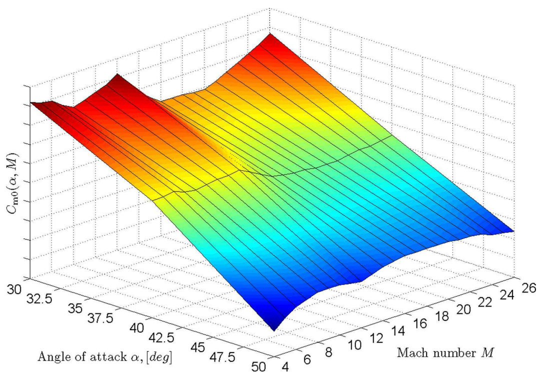

(a) C_{m0}

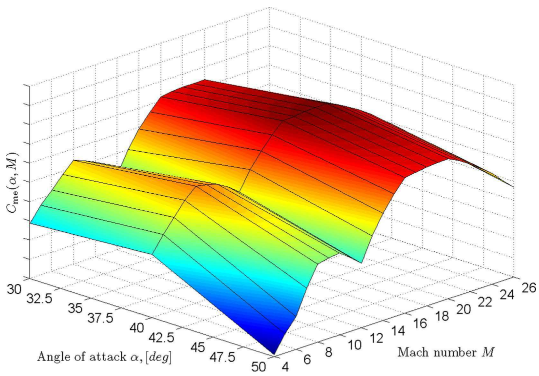

(b) C_{me}

Figure 4.11: Vehicle aerodynamic functions

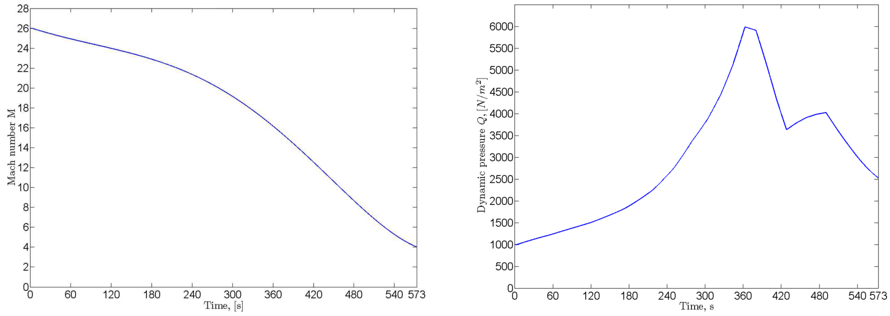

(a) *Mach number M* **(b)** *Dynamic pressure Q*

Figure 4.12: Time profiles for *M*, *Q*

The elevator fins are driven by an actuator that can be modeled as a second order filter governed by the following I/O representation:

$$\frac{d^2\delta_\mathrm{e}}{dt} + 2\xi\omega_\mathrm{a}\frac{d\delta_\mathrm{e}}{dt} + \omega_\mathrm{a}^2\delta_\mathrm{e} = \omega_\mathrm{a}^2\delta_\mathrm{c}. \tag{4.56}$$

4.2.2 Trim Analysis

`Trim control`

The first step of the *LBGS* procedure (trim control computation) is detailed in this section. The trim control $\delta_\mathrm{e}(\varrho_\mathrm{r}) = \delta_\mathrm{e,r}$ maintains the vehicle at a desired angle of attack in the absence of external perturbations. Of course since the Mach number varies according to the profile of Fig. 4.12a this control is not sufficient to stabilize the vehicle and a feedback control should be added. The trim control can be calculated as a function of the scheduling vector ϱ by supposing that at an equilibrium or reference state is imposed and consequently $\frac{dq}{dt}\big|_\mathrm{r} = 0$. To compute $\delta_\mathrm{e,r}$, Eq. 4.53-4.54 are used and the trim surface is obtained (Fig 4.13):

$$\delta_\mathrm{e}(\varrho_\mathrm{r}) = -\frac{C_\mathrm{m0}(\varrho_\mathrm{r})}{C_\mathrm{me}(\varrho_\mathrm{r})}. \tag{4.57}$$

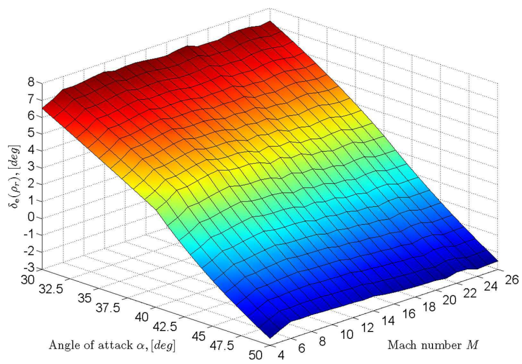

Figure 4.13: Vehicle trim control surface

4.2.3 System Linearization

4.2.3.1 LTI Models

LTI models

Having parameterized the system in terms of a scheduling vector ϱ, the second step of the (LBGS) procedure is to obtain LTI models of the vehicle for every desired operating point inside the flight envelope $\mathbf{\Gamma}_{\text{fe}}^{[\alpha,M]}$. Similarly to the procedure used for the missile, a family of linear models $\mathcal{S}_{\text{LPV}}(\varrho_{\text{r}})$ for every ϱ_{r} can be written in the following state space form:

$$\mathcal{S}_{\text{LPV}}(\varrho_{\text{r}}) \overset{\text{ss}}{:} \quad \dot{x}_\delta = \mathbf{A}(\varrho_{\text{r}})x_\delta + \mathbf{B}(\varrho_{\text{r}})\delta_{e,\delta} \tag{4.58}$$

with $x = [\alpha\ q]^T$ and:

$$x_\delta = x - x(\varrho_{\text{r}}) \tag{4.59}$$

$$\delta_{e,\delta} = \delta_{\text{e}} - \delta(\varrho_{\text{r}}). \tag{4.60}$$

The linearized matrices $\mathbf{A}, \mathbf{B}$ are given by:[13]

$$\mathbf{A}(\varrho_{\text{r}}) = \begin{pmatrix} 0 & 1 \\ \nabla_{\alpha,\text{r}} f_q & 0 \end{pmatrix} \tag{4.61}$$

$$\mathbf{B}(\varrho_{\text{r}}) = \begin{pmatrix} 0 \\ \nabla_{\delta_{\text{e}},\text{r}} f_q \end{pmatrix} \tag{4.62}$$

Jacobians

with:[14]

$$\nabla_{\alpha,\text{r}} f_q = \frac{SlQ_{\text{r}}}{I_{\text{yy}}} \left[\frac{\partial C_{\text{m0}}(\varrho_{\text{r}})}{\partial \alpha} - \frac{\partial C_{\text{me}}(\varrho_{\text{r}})}{\partial \alpha} \frac{C_{\text{m0}}(\varrho_{\text{r}})}{C_{\text{me}}(\varrho_{\text{r}})} \right] \tag{4.63}$$

$$\nabla_{\delta_{\text{e}},\text{r}} f_q = \frac{SlQ_{\text{r}}}{I_{\text{yy}}} C_{\text{me}}(\varrho_{\text{r}})\,. \tag{4.64}$$

The family of LTI systems $\mathcal{S}(\varrho_{\text{r}})$ is written in transfer function form:

$$\mathcal{S}(\varrho_{\text{r}}) \overset{\text{tf}}{:} \quad \left\{ \begin{bmatrix} \alpha_\delta(s) \\ q_\delta(s) \end{bmatrix} = \begin{bmatrix} G_\alpha(s) \\ G_q(s) \end{bmatrix} \delta_{\text{e},\delta} = G(s)\delta_{\text{e},\delta} \right. \tag{4.65}$$

where:

$$G(s) = \begin{bmatrix} G_\alpha(s) \\ G_q(s) \end{bmatrix} = \frac{1}{s^2 + \omega_0^2} \begin{bmatrix} b \\ bs \end{bmatrix}. \tag{4.66}$$

The corresponding natural frequency ω_0 and open loop gain b of the linear systems are calculated from the matrix elements A_{21}, B_{21} and vary as a function of the scheduling vector:

$$\omega_0^2(\varrho_{\text{r}}) = -\nabla_{\alpha,\text{r}} f_q \tag{4.67}$$

$$b(\varrho_{\text{r}}) = \nabla_{\delta_{\text{e}},\text{r}} f_q. \tag{4.68}$$

[13] The function $f_q : \mathbb{R}^3 \to \mathbb{R}$ is the right hand side of Eq. 4.53.

[14] The dynamic pressure Q is not considered as a scheduling parameter since it depends directly on the Mach; however the corresponding reference value Q_{r} is shown in the linearization equations.

4.2.3.2 Stability Analysis

A stability analysis of the vehicle dynamics is given here, based on the family of LTI models $\mathcal{S}_{\mathrm{LPV}}(\varrho_{\mathrm{r}})$ calculated for every value of the scheduling vector ϱ inside the vehicle flight envelope. It may be observed (e.g. from Eq. 4.65) that the linear models present two complex conjugate eigenvalues with zero real parts; thus the vehicle is *conditionally stable*.

Stability discussion

The three element surfaces $A_{12}(\varrho_{\mathrm{r}})$, $B_{12}(\varrho_{\mathrm{r}})$ and $\omega_0^2(\varrho_{\mathrm{r}})$ are visualized in Figs. 4.15a-4.15c. The first two figures presenting the evolution of the LTI matrix elements do not give more information further than underlining the heavy change of the system dynamics for all values of ϱ. However, Fig. 4.15c showing the form of the LTI models natural frequency dependence on ϱ, is particularly interesting. This is because a closed loop controller (namely a gain-scheduled one) should be able to maintain appropriate damping to the imaginary closed loop poles and also sufficient stability margins despite this dependence.

This 'bell' type surface is a very good way to characterize the variation of the system's dynamics and will also give rise to the discussion of Chapter 6 concerning gain scheduling control laws and their ability to *capture the plant's nonlinearities and change of dynamics*; it will indeed be shown that the gain-scheduled control laws calculated in Chapter 6 achieve this task by means of the gap metric.

This change of the natural frequency ω_0 can be also visualized in the following figure (Fig. 4.14) representing Bode magnitude diagrams of transfer functions G_α of the vehicle's family linear systems $\mathcal{S}_{\mathrm{LPV}}(\varrho_{\mathrm{r}})$ for a significant number of frozen values for ϱ.

As a last comment it can be said that whereas in the missile the pitch rate q is used also as a measured output; here it is not the case and only the angle of attack α is used. This is done primarily for reasons of simplicity of the feedback loop as it will be seen in the following chapters since a gain-scheduled controller of the least possible complexity is always sought.

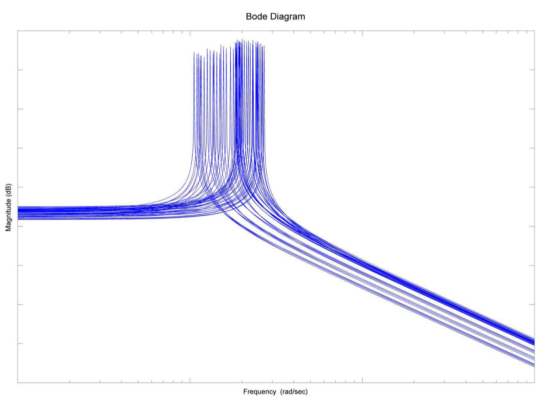

Figure 4.14: Vehicle Bode magnitude diagrams

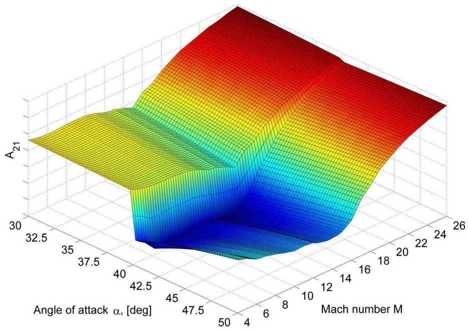

(a) *Element* A_{21}

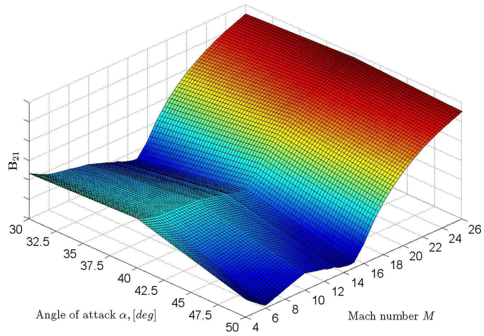

(b) *Element* B_{21}

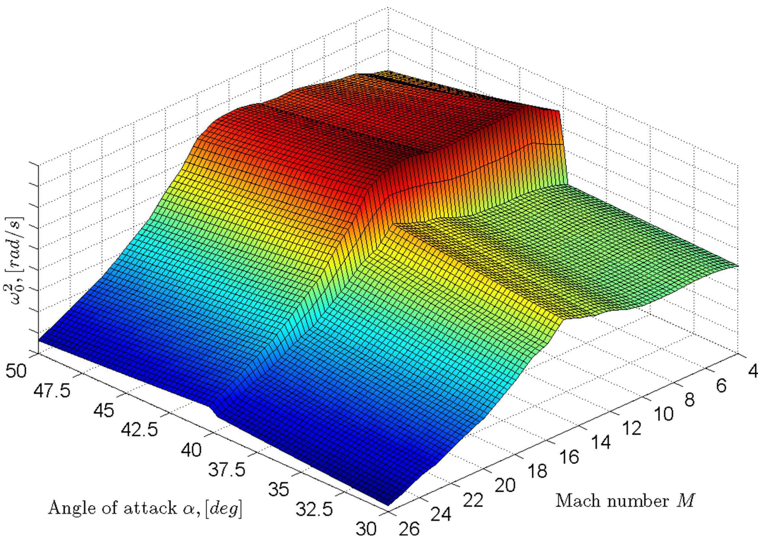

(c) *Natural frequencies*

Figure 4.15: Vehicle linearization results

4.3 Conclusions

In this chapter we have presented the preliminary work conducted concerning the modeling and analysis of the two benchmark systems used during the thesis in order to validate the proposed gain scheduling strategies of the following chapters. This phase practically corresponds to the first two steps of the LBGS procedure detailed in Section 1.3.1, namely the trim analysis (or equilibrium point parametrization) and the Jacobian linearization of the plants.

The procedure followed is similar in both cases: first choose a family of system variables (scheduling vector) to parameterize the equilibrium points of the initial nonlinear system and then use either symbolical or numerical techniques to calculate a trim control in order to equilibrate the state/output of the plant to a pre-defined desired value for all the operating domain of the system. Second, calculate LTI models of the system for a family of reference values of the scheduling vector and analyze their stability.

It has been analyzed that for the missile this parametrization is *output*-based whereas for the missile is *state*-based. The missile presents a small unstable region of its flight envelope whereas the vehicle is everywhere between the limits of stability and instability.